RSC Advances

PAPER

View Article Online
View Journal | View Issue

Cite this: *RSC Adv.*, 2016, **6**, 46984

Design of lipidic platforms anchored within nanometric cavities by peptide hooks†

G. M. L. Messina,[a] M. De Zotti,[b] R. Lettieri,[c] E. Gatto,[c] M. Venanzi,*[c] F. Formaggio,[b] C. Toniolo[b] and G. Marletta*[a]

Stable confinement of liposomes within arrays of hybrid polymer/Au nanocavities was achieved using peptide hooks covalently linked to the Au floor. The peptide hooks are thiolated analogs of trichogin GA IV (SSTrGA), a well-known broad-spectrum antimicrobial peptide with a high affinity for lipids, functionalized at the N-terminus with an α-lipoic group for linking to Au substrates. SSTrGA promoted opening of the liposomes, giving rise to the formation of a lipid bilayer paving the nanocavity. A patterned nanoporous surface was prepared using a colloidal solution of monodisperse silica nanospheres that formed a cubic close-packed array on the Au substrate. The nanosphere array was then processed using spin coating of a poly(methyl methacrylate) solution, followed by selective removal of the silica nanoparticles, yielding an array of hybrid nanocavities formed with poly(methyl methacrylate) walls and paved with an Au floor. The Au layer was then modified through covalent linkage to SSTrGA, forming a densely packed self-assembled monolayer on the Au floor of the nanowells, as demonstrated using cyclic voltammetry experiments. Atomic force microscopy and a quartz crystal microbalance with dissipation monitoring were used to study the inclusion of the peptide/liposome system in the hybrid nanocavities and the formation of the lipid bilayer inside them. This system could be usefully exploited as a patterned biomimetic environment able to host membrane proteins or lipophilic enzymes for the development of new bioinspired functional materials and for biosensing based on ligand–protein recognition.

Received 7th March 2016
Accepted 19th April 2016

DOI: 10.1039/c6ra06054d

www.rsc.org/advances

Introduction

The fabrication of nanopatterned surfaces is of great interest in the area of life sciences, due to their size-dependent properties, leading to a wide range of potential applications from bio- and chemical-sensors at the nanoscale level to the development of techniques to manipulate biological processes at the subcellular level, and to methodologies to obtain new nanostructured, intrinsically biocompatible coatings.[1–5]

A wide variety of techniques, conventionally classed as top-down and bottom-up techniques, are currently available to fabricate nanostructured surfaces. Among these, it is worth noting that while top-down methodologies, including photo-, electron- and ion-beam lithographies, are able to produce structures with dimensions far below 100 nm,[6–9] they suffer from the considerable drawbacks of demanding, complex, serial and cost-consuming processes, mostly suitable for small area treatments.

Alternatively, recent research has highlighted the advantages of using self-assembly processes operating in a parallel way, and this is the most promising for achieving large area surface nanostructuring. Among the various successful methodologies, the self-organization of colloidal nanoparticles on surfaces has been demonstrated to produce 2D and 3D nanotemplates, allowing the obtainment of a large number of nano-architectures with diverse functionalities.[10,11] These methods, globally indicated as colloidal crystal lithography (CL),[12–14] have been shown to be particularly suitable for biocompatible surface fabrication, through the inherent possibility of combined control of both the surface chemistry and topography.

The idea of confining biomolecules in nanosized structures is linked to the basic underlying assumption that nano-confinement affects the way biomolecules are organized/structured at surfaces, including their orientation,[15] their native or denatured state,[16] their aggregation propensity, and in turn their biological performance. Furthermore, the use of hybrid nanostructures would allow for modulation of the topography

[a]*Laboratory for Molecular Surfaces and Nanotechnologies (LAMSUN), Department of Chemical Sciences, University of Catania, Center for Colloids and Surface Science (CSGI), 95129 Catania, Italy. E-mail: gmarletta@unict.it*

[b]*ICB Padova Unit, CNR, Department of Chemistry, University of Padova, 35131 Padova, Italy*

[c]*Department of Chemical Sciences and Technologies, University of Rome "Tor Vergata", CSGI, 00133 Rome, Italy. E-mail: venanzi@uniroma2.it*

† Electronic supplementary information (ESI) available: Cyclic voltammetry blocking experiment of $K_3Fe(CN)_6$ using a bare Au electrode or a poly(methyl methacrylate)/Au substrate as the working electrode. See DOI: 10.1039/c6ra06054d

and chemistry at the nanometric scale, providing a breakthrough in the construction of smart biofunctional surfaces. In this context, particular attention has been paid to the preparation of surfaces bearing phospholipid bilayers, in view of the outstanding interest in them as models of cellular membranes as well as their potential for naturally biocompatible platforms.[17,18]

Of particular interest, among the various phospholipids, is 1-palmitoyl-2-oleoyl-*sn*-glycero-3-phosphocholine (POPC), because of the interest in its use in membrane models and its presence in eukaryotic cell membranes.[19,20]

In this study, we describe a versatile approach used to build a biomimetic platform, formed of polymeric cavities of nanometric size containing a lipid bilayer, stably anchored to the gold substrate paving the nanocavity (NC) by a thiolated peptide. Specifically, we use monodisperse silica nanospheres embedded within a poly(methyl methacrylate) (PMMA) ultrathin film layered on a gold substrate as the templating system. On removing the embedded template nanoparticles from the PMMA film, an array of hybrid NCs is formed, each NC consisting of polymeric walls and paved with an Au floor.

We also describe the synthesis of a peptide analog of trichogin GA IV, Oct-Aib-Gly-Leu-Aib-Gly-Gly-Leu-Aib-Gly-Ile-Lol (where Oct is 1-octanoyl, Aib is α-aminoisobutyric acid, and Lol is leucinol), an antimicrobial peptide with high affinity for the lipid phase.[21–23] In particular, we replaced its N-terminal Oct group with α-lipoic acid, to exploit the great affinity of a lipoic disulfide group for Au (~40 kcal mol^{-1}).[24] We will show that the N^{α}-lipoylated, Leu^{11}–OMe (where –OMe is methoxy) trichogin GA IV analog, denoted as SSTrGA, forms a densely packed self-assembled monolayer (SAM) on the Au floor of the nanocavity. The strong affinity of SSTrGA for lipids was then exploited to obtain stable confinement of POPC in the nanocavity. It is found that POPC liposomes are efficiently and stably included in the NCs coated with the SSTrGA SAM as a lipid bilayer, mimicking a biomembrane environment.

The formation of a peptide SAM, as well as the immobilization of the liposome bilayers in the nanocavities, is demonstrated using cyclic voltammetry (CV), atomic force microscopy (AFM), a quartz crystal microbalance with dissipation monitoring (QCM-D) and X-ray photoelectron spectroscopy (XPS). Using this approach, we obtain information on the peptide/liposome interaction as well as on the most suitable conditions for liposome immobilization.

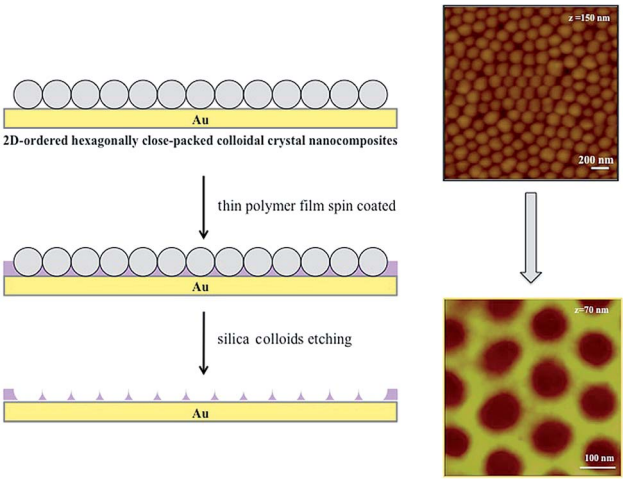

Fig. 1 Schematic representation of the procedure applied for the preparation of the nanocavity array (PMMA on Au). End of the top and bottom lines: AFM images of the NP array and of the final NC array on the Au surface.

Experimental

Substrate preparation

Au-coated silicon wafers were obtained from Sigma, cleaned using a basic piranha solution (a 5 : 1 : 1 mixture of water, concentrated ammonium hydroxide and 30% hydrogen peroxide), rinsed with Milli-Q water (18.2 MΩ cm^{-1}), and dried in a stream of nitrogen. NC arrays were prepared using the three-step procedure shown in Fig. 1. In the first step, an aqueous colloidal solution of silica nanoparticles ($\phi = 150$ nm) was spin-coated onto an Au surface, forming an ordered array of nanocrystals. The thickness of the resulting colloidal nanoparticle film was determined from the particle size, colloidal concentration, spin speed, and number of cycles in the spin-coating process. The packing of the colloidal nanoparticles was optimized by means of a subsequent mild annealing at 90 °C, promoting the formation of a close-packed 2D colloidal crystal structure. The self-organization of the silica nanoparticles is ruled by slightly repulsive intermolecular forces, related to the hydrophilic anionic character of the nanoparticle surface. Nanoparticle (NP) arrays appeared, ensuring a homogeneous covering of the large areas of the substrates.

A thin layer of PMMA was then spin coated on the NP array, forming a filling layer, the thickness of which can be efficiently tuned by modulating the polymer concentration and the spin rate. Finally, the NPs were removed by selective etching with HF, leaving behind a 2D-ordered array of polymeric NCs supported on Au.

The resulting NCs have, therefore, PMMA walls and a conductive Au floor. AFM images of the NP array on the Au surface and of the final NC array are shown at the ends of the top and bottom lines of Fig. 1, respectively. The average depth of the NCs was found to be 39 ± 2 nm and the average diameter about 97 ± 8 nm.

Liposome preparation

An appropriate amount of POPC, 10 mg mL^{-1} $CHCl_3$ solution, purchased from Avanti Polar Lipids (Alabaster, AL) was poured into an evaporation flask. Lipid films were obtained by evaporation of the $CHCl_3$ under reduced pressure and storage under vacuum overnight. The resulting phospholipid film was hydrated with a 10 mM phosphate buffer (pH 7.4), containing 140 mM NaCl and 0.1 mM EDTA, to afford a 10 mM phospholipid solution. This solution was vortex-mixed and then freeze-thawed ten times, from liquid nitrogen temperature to 313 K. The lipid dispersion was extruded 31 times through two stacked polycarbonate membranes with 100 nm pores (Avestin, Ottawa,

Ontario, Canada), to obtain uniform sized-monodispersed vesicles. The final phospholipid concentration was determined using the Stewart method. A 1 mM liposome solution was kept in contact with a NC-structured substrate for 18 h.

Peptide synthesis

The preparation and characterization of the synthetic precursor of SSTrGA, Z-Aib-Gly-Leu-Aib-Gly-Gly-Leu-Aib-Gly-Ile-Leu-OMe (where Z is benzyloxycarbonyl), are reported in ref. 25. After N^{α}-deprotection *via* catalytic hydrogenolysis, the N-terminal free peptide ester was acylated with commercial (Sigma-Aldrich, St. Louis, MO) (*R*,*S*)-α-lipoic acid[26,27] using *N*-ethyl-*N*′-(3-dimethylaminopropyl)carbodiimide hydrochloride and 1-hydroxy-7-azabenzotriazole.[28] Reaction of the racemic α-lipoic acid with the chiral 11-mer peptide ester afforded a mixture of two SSTrGA diastereomers. SSTrGA characterization: mp: 176–177 °C. IR (KBr): 3313, 1738, 1655, 1538 cm^{-1}. $[\alpha]_D$: −18.6 (c = 0.5, CH_3OH). ESI-MS: $[M + H]^+$ calcd = 1156.6396; $[M + H]^+$ found = 1156.6382. The chemical structures and acronyms for the compounds used in this work are shown in Scheme 1.

Cyclic voltammetry (CV)

CV data were obtained using a PG-310 potentiostat (HEKA Elektronik, Lambrecht, Germany) at room temperature. A standard three-electrode configuration was used with a PMMA-coated Au electrode as the working electrode, a platinum wire as the auxiliary electrode and an Ag/AgCl electrode as the reference. A 0.5 mM $K_3Fe(CN)_6$ aqueous solution in 1 M KCl was used as the electroactive component in the blocking experiment and the sweep rate was set at 50 mV s^{-1}.

Quartz crystal microbalance with dissipation monitoring (QCM-D)

Adsorption kinetics measurements were obtained using a QCM-D instrument (Q-Sense E1, Biolin Scientific Sweden) with AT-cut Au crystals covered by the spin-coated polymer film and operating in Millipore water at 25 ± 0.1 °C. The measurement cell had a volume of 40 μL and simultaneous measurements of the frequency, F, and energy dissipation, D, were performed for the fundamental resonance frequency (n = 1, *i.e.* F = 5 MHz) and the first three overtones (n = 3, 5, and 7, corresponding to F = 15, 25, and 35 MHz, respectively). In the case of a rigid adsorbed layer, the frequency to mass conversion was obtained by applying the Sauerbrey relation:[29] $\Delta m = -(C/n)\Delta F$, where ΔF is the decrease in the resonance frequency, Δm is the mass uptake at the sensor surface, C is a constant depending on the intrinsic properties of the quartz slab (in our case C = 17.7 ng cm^{-2} Hz^{-1} at F = 5 MHz) and n is the overtone number. The measurement accuracy for F and D is ±0.1 Hz and 1 × 10^{-6}, respectively.[30]

Each QCM-D experiment started with the sensor in water (out-gassed by 30 min of sonication under vacuum), followed by the addition of the lipid solution and, after 30 min, by the exchange of the lipid solution with Millipore water, to check both the desorption and stability of the adsorbed layer.

Atomic force microscopy (AFM)

AFM observations were carried out with a "J scanner" in tapping mode using a Nanoscope IIIA-MultiMode AFM (Digital Instruments, Santa Barbara, CA) at room temperature. The force was maintained at the lowest possible value by continuous adjusting of the set point during imaging. Images were recorded using 0.5–2 Ω cm phosphorous (n) doped silicon tips mounted on

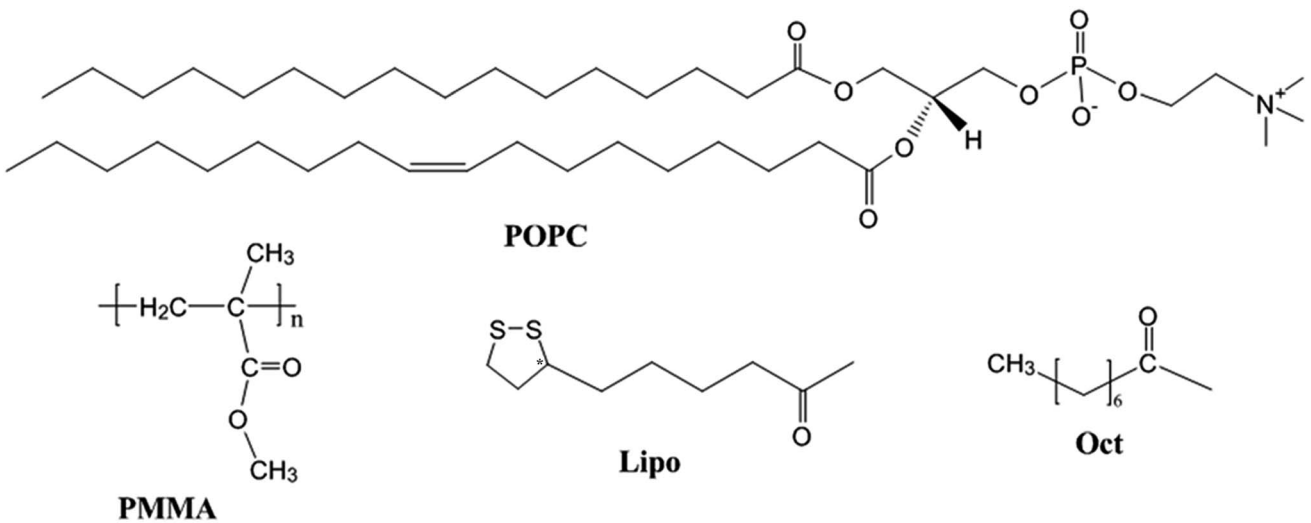

Lipo-Aib-Gly-Leu-Aib-Gly-Gly-Leu-Aib-Gly-Ile-Leu-OMe

SSTrGA

Scheme 1 Chemical structures and acronyms for the compounds used in this work.

cantilevers with a nominal force constant of 40 N m^{-1}, a resonance frequency of 300 kHz, and a tip curvature radius of 10 nm.

X-ray photoelectron spectroscopy (XPS)

Angular-dependent XPS (AD-XPS) measurements were performed using a small spot apparatus (AXIS-ULTRA Kratos), equipped with a hemispherical analyzer. Spectra were acquired at 90° and 20° photoelectron take-off angles (θ) with respect to the sample surface, in order to profit from the angle dependence of the sampling depth.[31] Accordingly, the thickness of the analyzed layer was evaluated using the relationship:

$$d\,(\mathrm{nm}) = 3\lambda\,(\mathrm{nm})\sin\theta \quad (1)$$

where λ (nm), the energy-dependent inelastic mean free path of the photoelectrons, was approximated to the attenuation length (AL) value of 3.48 nm for photoelectrons of 162.00 eV, *i.e.* corresponding to S 2p photoelectrons in organic layers.[32] The estimated sampling depth is 10.4 nm at 90° and 3.6 nm at a 20° take-off angle (θ). The X-ray source (Al K$\alpha_{1,2}$ at 1486.6 eV) was operated at a power of 15 kV and 10 mA, to minimize sample damage during the time required to acquire the full set of angle-dependent XPS data. The sample integrity was monitored by comparing the shape of the main peaks before and after spectra acquisition. The pressure in the analysis chamber was maintained at about 10^{-9} torr during the measurements. All binding energies were referenced to the C 1s neutral carbon peak at 285.0 eV.[32] A Shirley-type background was subtracted from each spectrum. The peak fitting analysis was performed using Gaussian curves with a constant full width at half-maximum (FWHM) for all components of a given peak.

Results and discussion

Ex situ analysis of SSTrGA and POPC liposome adsorption

Ex situ angle-dependent XPS measurements were carried out to investigate the interactions of SSTrGA with the bare Au and the PPMA substrates, and POPC with the bare Au, the SSTrGA-coated Au and the PPMA substrates. Fig. 2 shows the high-resolution peak shapes of C 1s, N 1s and S 2p, respectively, for the SSTrGA-coated Au (Fig. 2a–c) and PMMA surfaces (Fig. 2d–f). Owing to the lack of characteristic S 2p and N 1s peaks, it is clear that the SSTrGA peptides do not adsorb at all onto the PMMA surfaces, which only exhibit the simple C 1s band shape characteristic of the polymer.

In contrast, the N 1s and S 2p peaks found for the SSTrGA-coated Au surfaces indicate that the lipoylated molecules have been efficiently adsorbed, as confirmed from detailed analysis of the S 2p and N 1s regions. Actually, the S 2p region shows two peaks, respectively at a binding energy (BE) of 161.9 ± 0.2 eV and 163.1 ± 0.2 eV, corresponding to the well-resolved spin orbit coupling components of the S 2p peak, with the characteristic $2p_{3/2}$–$2p_{1/2}$ doublet separation of 1.2 eV and the 2 : 1 area ratio. The $2p_{3/2}$ BE closely corresponds to that typical for a covalent S–Au linkage.[33] The single binding state found for the S atoms confirms that all the lipoic acid units are involved in S–Au bonding interactions, suggesting in turn that all the SSTrGA molecules are linked to the Au substrate. The N 1s peak shows a well-defined single component at 400.2 ± 0.2 eV, assigned to the amide linkage.[34,35] The BEs and relative intensities of the components of the C 1s band, at 285.1 ± 0.2 eV for the C–C and C–H bonds, at 286.6 ± 0.2 eV for the C–O and C–N bonds, and at 288.2 ± 0.2 eV for the C═O groups, closely reflect the chemical formula of SSTrGA.

Furthermore, an angular dependent analysis indicated that the intensities of the C 1s and N 1s peaks, the latter being a particular marker of the peptide presence, increase about 1.5 times in the surface-enhanced mode with respect to the bulk-mode spectra, suggesting that the N-containing groups are oriented outwards. In contrast, the apparent intensities of the S 2p and O 1s peaks remain roughly constant in the surface-enhanced mode, suggesting that the lipoic units of the SSTrGA molecules, including both dithiolanes and carbonyl groups, are positioned at the very interface between the peptide and the Au substrate.

Fig. 3 illustrates the high-resolution XPS spectra for POPC adsorbed onto the bare Au, PMMA, and SSTrGA-Au surfaces. It can be seen that the POPC liposomes are quite efficiently adsorbed on the bare Au surface (Fig. 3a), as this is apparent from the N 1s and P 2p peaks. In particular, the high resolution N 1s peak is found at BE = 402.1 ± 0.2 eV, corresponding to the BE of a quaternary nitrogen atom, as expected for POPC. Surface enhanced spectra (not reported here) showed an increase of the P 2p and a reduction of the N 1s peak intensities in the sampled outer POPC layers. These findings suggest that the interaction between POPC and the Au surface is indeed mediated by the quaternary nitrogen atom oriented towards the latter.

The XPS data for the PMMA surfaces exposed to the POPC solution (Fig. 3b) clearly show that no significant adsorption occurs in this case.

Finally, the XPS spectra for the POPC/SSTrGA/Au surface (Fig. 3c) highlight the peculiar signature of the adsorbed POPC vesicles and the SSTrGA layer. Indeed, the C 1s and N 1s percentages for these surfaces are slightly higher than those for the SSTrGA/Au surfaces, while the signal of S 2p at the SSTrGA/Au interface is below the detection limit, suggesting that the adsorbed POPC vesicles form an efficient attenuating overlayer on the SSTrGA film. Accordingly, the surface-enhanced spectra (at 20 °C) show an increased P 2p peak, indicative of the occurrence of POPC phosphate groups at the surface of the overlayer, *i.e.* on top of the SSTrGA layer. On the other hand, the BE of the N 1s peak, 400.2 ± 0.2 eV, corresponding to the amide nitrogen atom in SSTrGA, as well as its high intensity, very close to those measured for SSTrGA/Au surfaces, confirm that the peptide molecules form an intermediate layer between POPC and the Au substrate.

In situ analysis of the POPC liposome adsorption

The interaction of the POPC liposomes, in a phosphate buffer saline (PBS) solution, with a bare Au surface and an Au surface coated by the SSTrGA SAM was preliminarily investigated using QCM-D measurements. In Fig. 4a the frequency variation ΔF

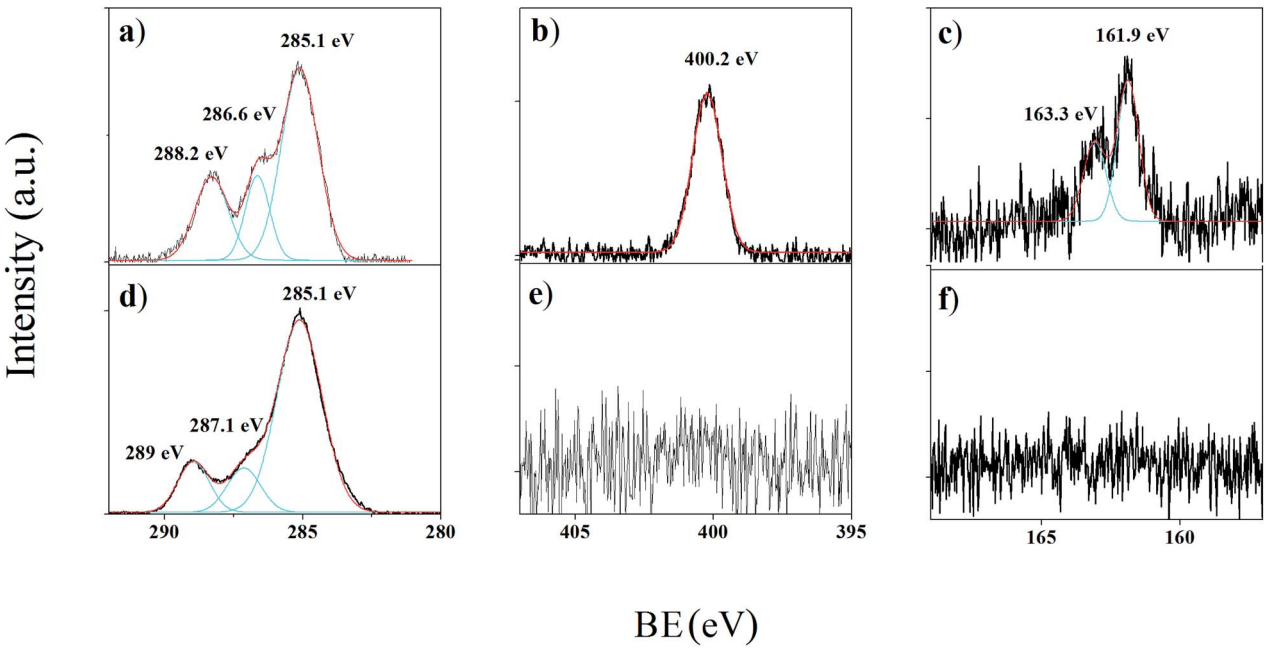

Fig. 2 XPS C 1s (left), N 1s (middle), and S 2p (right) peaks of SSTrGA adsorbed on different surfaces: (a–c) the bare Au surface and (d–f) the PMMA film.

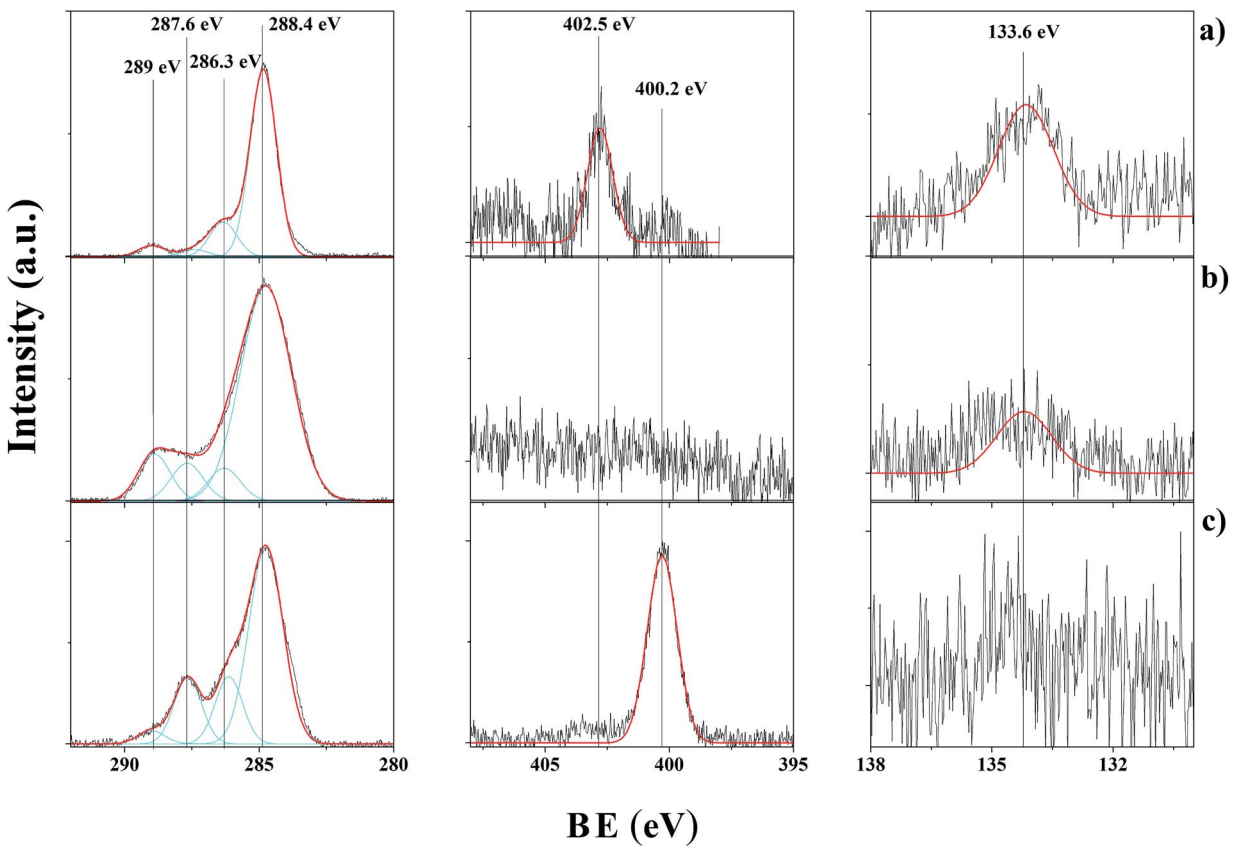

Fig. 3 XPS C 1s (left), N 1s (middle), and P 2p (right) peaks of POPC adsorbed on different surfaces: (a) bare Au; (b) PMMA film, and (c) SSTrGA SAM on the Au surface.

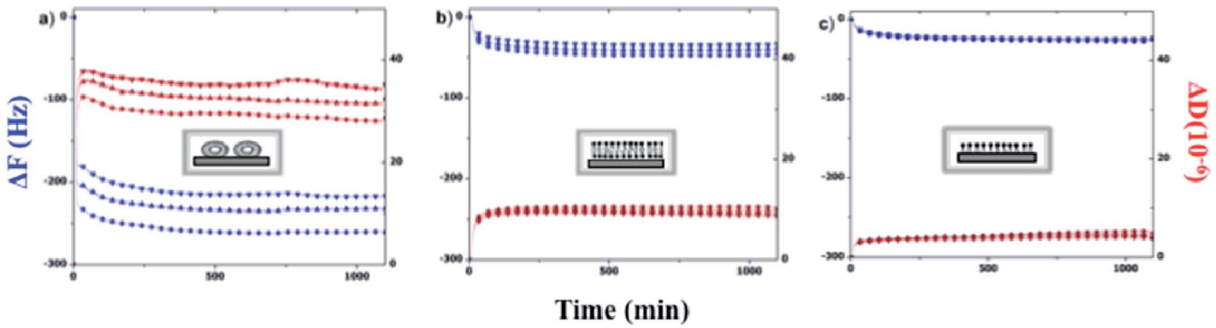

Fig. 4 QCM-D measurements for POPC liposome deposition on: (a) an Au surface; (b) an Au surface modified by chemisorption of a SSTrGA SAM; (c) a PMMA substrate.

and the change of the dissipation factor ΔD upon immobilization of POPC liposomes on the Au substrate are reported. Large shifts of both the resonant frequency ($\Delta F = -236.8$ (± 22.3) Hz) and the dissipation factor ($\Delta D = 32.0$ (± 3.4) $\times$ 10^{-6}) are seen. In agreement with the literature,[36] this behavior, characterized by a peculiar monotonic decrease in frequency until the equilibrium is reached and a very large dissipation shift, is attributed to the adsorption of intact lipid vesicles, taking into account the mass of the buffer entrapped either within the vesicles or between the vesicles and the surface. The large dissipation, in particular, is typical of adsorbed vesicles, owing to their large deformations under shear stress.[37] This conclusion is further supported by the large spread of values across the three overtones, which is a signature of the large vertical inhomogeneity of the adsorbed systems, as expected for the complex interplay of vesicles and entrapped water. Indeed, the QCM-D signal is produced from three (3^{rd}, 5^{th} and 7^{th}) overtones, the penetration depth of which is progressively decreasing with the increasing overtone number.[38]

In summary, the adsorption of intact vesicles indicates that the interaction forces between the lipid vesicles and the Au surface are not strong enough to cause vesicle rupture. In contrast, the adsorption of POPC liposomes on a SSTrGA SAM layer covalently linked to the Au surface (Fig. 4b) gives rise to a fast mass uptake followed by an equilibrium state at relatively low frequencies ($\Delta F = -39.1 \pm 6.0$ Hz). The dissipation of the adsorbed layer is quite low ($\Delta D = 9.3 \pm 0.8 \times 10^{-6}$) and the three overtones are remarkably close, suggesting a vertically homogeneous adsorbed layer, *i.e.* the occurrence of a fast adsorption-and-rupture process for the vesicles. Accordingly, this result provides strong evidence that the self-assembled peptide layer induces a straightforward opening of the liposome as it approaches the SSTrGA-coated surface, giving rise to formation of a lipid bilayer characterized by a relatively high rigidity and vertical homogeneity (Fig. 4b).

Control QCM-D experiments concerning the adsorption of POPC onto a PMMA thin film (Fig. 4c), show that a lower mass was adsorbed, $\Delta F = -24.7 \pm 1.7$ Hz, with a comparably low dissipation $\Delta D = (4.1 \pm 0.5) \times 10^{-6}$ (*i.e.* high rigidity). The fact that the adsorbed vesicle mass and the dissipation factor roughly correspond to half of the values measured for POPC bilayers adsorbed onto the SSTrGA-coated surfaces suggests that random monolayer domains are formed on the PMMA surfaces.

POPC liposome adsorption within nanocavities

The nanostructured films consisting of ultrathin PMMA layers with arrays of nanocavities were exposed to SSTrGA and POPC. According to the above reported results, it was expected that both SSTrGA and POPC would not be adsorbed onto the PMMA area, but rather located within the Au floor of the nanowells.

CV experiments were performed using the nanostructured PMMA/Au surface as the electrode. We obtained the effective electrode surface accessible to a redox active compound by quantifying the discharge of an electrochemical reference. CV spectra recorded using a PMMA film on Au or a PMMA/Au NC array as the working electrode in the presence of potassium ferricyanide show that for the first system no ferricyanide discharge could be measured, indicating that the substrate is homogeneously and completely covered by the PMMA passivating layer (ESI†). In contrast, for the nanostructured array of nanocavities within the PMMA film, typical reduction and oxidation peaks, associated with ferricyanide discharge, can be observed (Fig. 5). Incidentally, this finding confirms the accessibility of the NC Au floor to the electrolyte. A substantial decrease of the CV signal is generally observed when an insulating layer passivates the Au electrode.

This decrease would depend on the degree of coating of the Au surface, the absence of defects in the insulating layer, and its packing density. In Fig. 5, we show the CV spectra obtained in the presence of potassium ferricyanide, using the Au/PMMA NC array as the working electrode and the same nanostructured

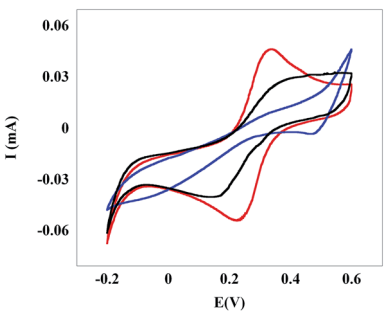

Fig. 5 CV spectra of the discharge of ferricyanide ions on a PMMA/Au nanocavity platform before (red) and after 5 min (blue) and 18 h (black) of incubation in a millimolar POPC solution.

support incubated for 5 min or 18 h in a millimolar POPC solution. Interestingly, it can be observed that the reduction and oxidation bands centered at $E_0 = 0.25$ V are strongly depleted in the case of the short-time incubation with the liposome solution. However, for longer incubation times (18 h), the discharge of the $[Fe(CN)_6]^{3-}/[Fe(CN)_6]^{4-}$ redox pair on the Au/PMMA/POPC working electrode occurs with a relatively high intensity.

This finding suggests the selective inclusion of liposomes in the PMMA NCs, which is eventually subjected to a liposome-to-lipid bilayer transition occurring at relatively longer incubation times. The latter phase is characterized by a relatively high permeability of ferricyanide or small ions, giving rise to both faradaic and capacitive current contributions.

On the contrary, when the same experiment was repeated using an NC platform as the working electrode, previously incubated overnight in a millimolar SSTrGA solution, the electroactivity of ferricyanide was almost completely inhibited (Fig. 6).

This result indicates the formation of a densely packed peptide SAM on the Au floor of the etched PMMA/Au substrate, passivating the Au floor of the NCs toward ferricyanide discharge.

To exploit the high affinity of trichogin GA IV for lipid formulations and its ability to anchor liposomes of a diameter matching the nanocavity size, CV experiments in the presence of the ferricyanide electrolyte were carried out on an Au/PMMA/SSTrGA platform incubated in a 0.5 millimolar solution of POPC liposomes with an average diameter of 100 nm. The results (Fig. 7) showed that, for the Au/PMMA/SSTrGA/POPC system, the ferricyanide discharge on the Au surface was almost completely restored (the CV curves obtained using Au/PMMA/POPC or Au/PMMA/SSTrGA working electrodes are also reported in Fig. 7 for comparison).

This finding suggests that the peptide SAM promoted the stable inclusion of the liposome in the NCs, and that peptide/liposome interactions enhance the permeability of the lipid layer and perturb the packing density of the peptide SAM, allowing for efficient $[Fe(CN)_6]^{3-}/[Fe(CN)_6]^{4-}$ discharge to the electrode.

This result can be readily explained considering the high antimicrobial activity of SSTrGA. Currently, the molecular

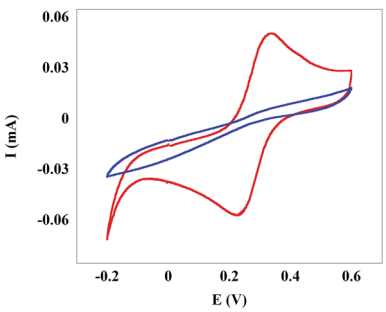

Fig. 6 CV spectra of the $[Fe(CN)_6]^{3-}/[Fe(CN)_6]^{4-}$ pair in the case of a bare NC platform (red) and of an NC array modified by deposition of a SSTrGA SAM (blue).

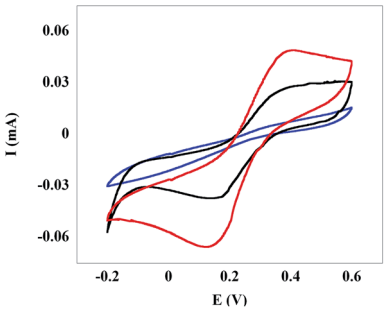

Fig. 7 CV spectra of the $[Fe(CN)_6]^{3-}/[Fe(CN)_6]^{4-}$ discharge in the case of an NC platform modified by deposition of a SSTrGA SAM (blue). In red, the CV curve obtained for the same SSTrGA-coated support, incubated for 18 h in a 0.5 millimolar liposome solution. For comparison, the CV curve measured in the case of an NC platform incubated for 18 h in a millimolar POPC solution (black) is also shown.

mechanism of the bioactivity of this peptide is under intense scrutiny and several models have been proposed in the literature.[22,23,39,40] According to the barrel stave model, SSTrGA should form permanent channels through the cell membrane, causing the cytoplasmic content to exit. Alternatively, the carpet mechanism hypothesizes a strong perturbation of the surface properties of the bilayer, inducing partial (transient pores) or total destruction of the membrane. Recently, an interesting contribution by Stella and coworkers[41] proved that trichogin GA IV binding to liposomes produces a decrease of the thickness of the bilayer, thus favoring the transit of ions and small molecules through the liposome layer. Similar results were also recently reported for the disruption of phospholipid membranes by amyloid fibers.[42]

The CV results reported earlier in the text, in close agreement with those for the selective adsorption of SSTrGA and POPC on the Au and PMMA surfaces, confirm the high affinity of SSTrGA for lipid formulations and its perturbation activity on the liposome phase structure. In our case, indeed, the binding of the peptide to the liposome has three main effects: (i) according to the described lack of POPC adsorption on the PMMA, it stably anchors the liposome in the NC; (ii) according to the QCM-D adsorption results, which suggest straightforward opening of the POPC vesicles into bilayers on the SSTrGA/Au surfaces, it promotes opening of the liposome to form a lipid bilayer; (iii) according to the CV evidence, it strongly perturbs the adsorbed phospholipid bilayer and the packing density of the peptide SAM, allowing the discharge of ions and small molecules to the Au electrode.

Finally, AFM experiments gave further insight into the modes of inclusion of the POPC liposomes in the Au/PMMA/SSTrGA platform. Fig. 8 shows a typical AFM image of the etched PMMA/Au platform before (Fig. 8a) and after deposition of a millimolar POPC solution with different incubation times (Fig. 8b). For a short incubation time (5 min), the inclusion of intact liposomes (100 nm diameter) in the NCs can be easily seen. Interestingly, some of the NCs appear to be completely filled by POPC, most likely by the intact POPC liposomes. However, from Fig. 8c it can be noted that after a long

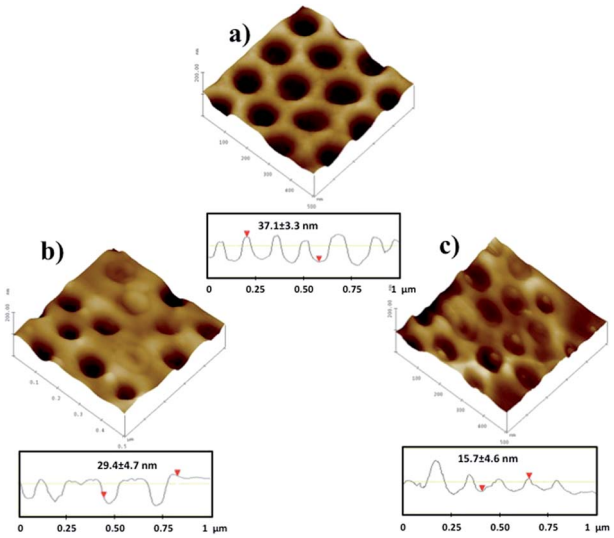

Fig. 8 AFM images of the etched PMMA/Au platform: (a) as obtained, and (b) after 5 min and (c) after 18 h of incubation in a millimolar POPC solution.

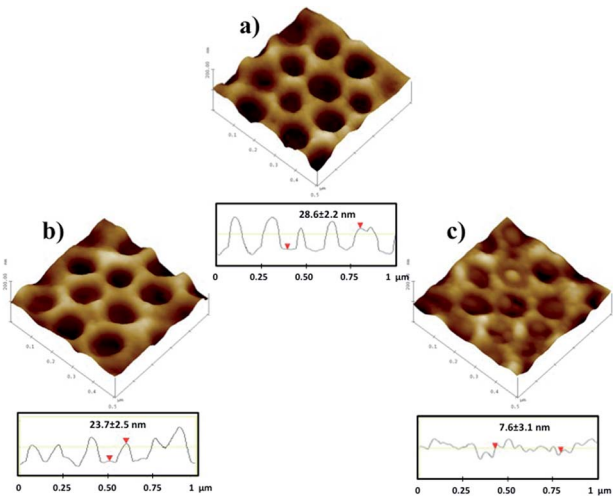

Fig. 9 AFM images of the nanopore array: (a) after 18 h incubation in a millimolar SSTrGA solution, and after a subsequent (b) 5 min and (c) 18 h of incubation in a millimolar POPC solution.

incubation time (18 h), only a few intact liposomes of somewhat smaller dimensions could be imaged from the AFM measurements.

The platform depth profiles, also shown in Fig. 8 below the associated images, indicate that the NCs of the etched PMMA/Au platforms have diameters of about 100 nm and depths of about 37 ± 3 nm. Also, the POPC-incubated NCs show variable depths of 29 ± 5 and 16 ± 5 nm for freshly incubated (5 min) and overnight (18 h) incubated samples, respectively. These data suggest that the initial adsorption of the intact liposomes is followed by a liposome-to-lipid bilayer transition, in agreement with point (ii) mentioned earlier in the text, and that the NCs are filled by lipid multilayers, each bilayer having an

Table 1 AFM measurements of the cavity depth for a bare NC array and peptide-coated NCs with or without inclusion of the liposome formulation

Sample	Pore depth (nm)
NC	37 ± 3
NC/POPC (before rinsing)	16 ± 5
NC/POPC (after rinsing)	28 ± 4
NC/SSTrGA	29 ± 2
NC/SSTrGA/POPC (before rinsing)	8 ± 3
NC/SSTrGA/POPC (after rinsing)	22 ± 5

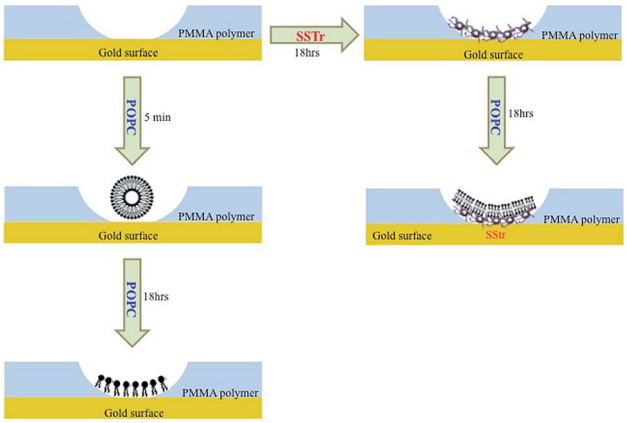

Scheme 2 Model of the liposome (POPC)/peptide (SSTrGA) interactions with the polymeric (PMMA) NC array.

average thickness of about 4 nm. These conclusions are in good agreement with the CV results illustrated in Fig. 5. No intact liposomes were seen on the upper smooth PMMA surface.

When the peptide SAM was allowed to interact with the etched Au/PMMA platform (Fig. 9a), its inclusion could not be directly imaged using AFM, due to the small thickness of the peptide monolayer (2 nm) with respect to the NC depth. However, a cross-sectional analysis of the NCs before and after exposure to SSTrGA shows that the depth of the NC decreases from 37 (±3) to 29 (±2) nm upon incubation of the bare NC platform with an SSTrGA millimolar solution, and to 24 (±2) nm when liposomes are allowed to interact with the SSTrGA-functionalized NC array. This result strongly supports the view that the NCs are partially filled by a POPC bilayer, "harpooned" into the NC using the SSTrGA peptide hooks.

Incubation of the Au/PMMA/SSTrGA platform for a long time (18 h) in a millimolar POPC liposome solution further reduces the depth of the NCs to 8 (±3) nm. This finding supports the view that POPC multilayers are adsorbed, filling almost completely the NCs. However, after rinsing, the NC depth increases to 28 and 22 nm, respectively, for the NC/POPC and NC/SSTrGA/POPC systems, suggesting that the merely physisorbed liposomes were removed from the NCs.

The average NC depths measured through AFM experiments on an NC array modified by chemisorption of a peptide layer

(NC/SSTrGA), and/or incubated in a millimolar liposome solution (NC/SSTrGA/POPC and NC/POPC), are summarized in Table 1.

As the peptide monolayer is about 2 nm thick and the POPC double layer is about 4 nm thick, we suggest that a liposome multilayer (2 or 3 bilayers) is adsorbed within the NC, but that stable inclusion of a POPC layer within an NC is only achieved with a SSTrGA monolayer immobilized on the Au floor, in agreement with our CV experiment results. Preliminary results on the stability of the liposome formulations embedded into the polymeric nanocavities, indicated that the NC/SSTrGA/POPC system is stable, at least, within a week from the liposome deposition. A schematic drawing for the proposed adsorption process is shown in Scheme 2.

Conclusions

XPS, QCM-D, CV, and AFM experiments unambiguously show that stable anchorage of lipid bilayers into polymeric patterned NCs can be obtained using peptide hooks covalently linked to an Au substrate. There are several ingredients that have made this design successful: (i) the production of patterned PMMA NCs starting from an ordered array of sacrificial silica NPs; (ii) a strong affinity of the lipoyl group of the peptide for the Au substrate, (iii) the inclusion/perturbation properties of the antimicrobial peptide (trichogin GA IV) employed for lipid anchoring and its strong affinity for lipids. As a result, we obtained patterned NCs hosting a lipid bilayer stably anchored at the bottom of the well.

Specific studies on the long-term stability of the hybrid systems investigated, and in particular on the different stability of NC/Au/liposome *vs.* NC/Au/SSTrGA/liposome, are being undertaken in view of their use as protein containers. Preliminary tests have indeed provided promising results.

It is now well-established that liposome formulations can be used for sensing and molecular recognition studies in a biomimetic environment, allowing retention of the native structures and functions of biomolecules.[43,44] Therefore, ordered arrays of lipid nanocontainers (such as the one described above) could allow study of the organization and properties of confined functional proteins on a nanometric scale, using electrochemical and optical methods. The ultimate goal is to obtain selective confinement of proteins in a friendly hosting environment, achieving single-protein sensitivity.[45]

Acknowledgements

Marta De Zotti and Grazia Maria Lucia Messina are grateful to MIUR (Rome, Italy) for financial support (Futuro in Ricerca 2013, grant no. RBFR13RQXM). Giovanni Marletta and Grazia Maria Lucia Messina acknowledge the financial support of FIR 2014 (University of Catania, Italy) and PRIN 2010–2011 (MIUR, Rome, Italy) for "Metodologie chimiche innovative per biomateriali intelligenti".

Notes and references

1 S. P. R. Kobaku, A. K. Kota, D. H. Lee, J. M. Mabry and A. Tuteja, *Angew. Chem., Int. Ed.*, 2012, **51**, 10109–10113.
2 J. Y. Lin, A. D. Stuparu, M. D. Huntington, M. Mrksich and T. W. Odom, *J. Phys. Chem. C*, 2013, **117**, 5286–5292.
3 K. H. A. Lau, J. Bang, C. J. Hawker, D. H. Kim and W. Knoll, *Biomacromolecules*, 2009, **10**, 10661–11066.
4 K. Kolind, K. W. Leong, F. Besenbacher and M. Foss, *Biomaterials*, 2012, **33**, 6626–6633.
5 J. T. Koepsel and W. L. Murphy, *ChemBioChem*, 2012, **13**, 1717–1724.
6 P. M. Mendes, S. Jacke, K. Critchley, J. Plaza, Y. Chen, K. Nikitin, R. E. Palmer, J. A. Preece, S. D. Evans and D. Fitzmaurice, *Langmuir*, 2004, **20**, 3766–3768.
7 Y. W. Su, C. S. Wu, C. C. Chen and C. D. Chen, *Adv. Mater.*, 2003, **15**, 49–51.
8 R. Sanz, M. Jaafar, M. Hernández-Vélez, A. Asenjo, M. Vázquez and J. Jensen, *Nanotechnology*, 2010, **21**, 235301.
9 K. Lu, C. Hammond and J. Qian, *J. Mater. Sci.*, 2010, **45**, 582–588.
10 S. H. Kim, S. Y. Lee, G. R. Yi, D. J. Pine and S. M. Yang, *J. Am. Chem. Soc.*, 2006, **128**, 10897–10904.
11 I. Karakurt, P. Leiderer and J. Boneberg, *Langmuir*, 2006, **22**, 2415–2417.
12 X. Yu, H. Zhang, J. K. Oliverio and P. V. Braun, *Nano Lett.*, 2009, **9**, 4424–4427.
13 M. M. Shindel, A. Mohraz, D. R. Mumm and S. W. Wang, *Langmuir*, 2009, **25**, 1038–1046.
14 L. Wang, L. Xia, G. Li, S. Ravaine and X. S. Zhao, *Angew. Chem., Int. Ed.*, 2008, **47**, 4725–4728.
15 H. Xu, X. Zhao, C. Grant, J. R. Liu, D. E. Williams and J. Penfold, *Langmuir*, 2006, **22**, 6313–6320.
16 J. R. Liu, S. Perumal, X. Zhao, F. Miano, V. Enea, R. R. Heenan and J. Penfold, *Langmuir*, 2005, **21**, 3354–3361.
17 I. Pfeiffer, S. Petronis, I. Koper, B. Kasemo and M. Zach, *J. Phys. Chem. B*, 2010, **114**, 4623–4631.
18 B. Garnier, S. Tan, C. Gounou, A. R. Brisson, J. Laroche-Traineau, M.-J. Jacobin-Valat and G. Clofent-Sanchez, *Biointerphases*, 2012, **7**, 11–19.
19 L. Huynh, N. Perrot, V. Beswick, V. Rosilio, P. A. Curmi, A. Sanson and N. Jamin, *Langmuir*, 2014, **30**, 564–573.
20 N. D. Duro, M. Gjika, L. Scott and S. Varma, *Biophys. J.*, 2015, **108**, 77a–78a.
21 C. Auvin-Guette, S. Rebuffat, Y. Prigent and B. Bodo, *J. Am. Chem. Soc.*, 1992, **114**, 2170–2174.
22 L. Stella, C. Mazzuca, M. Venanzi, A. Palleschi, M. Didonè, F. Formaggio, C. Toniolo and B. Pispisa, *Biophys. J.*, 2004, **86**, 936–945.
23 C. Mazzuca, L. Stella, M. Venanzi, F. Formaggio, C. Toniolo and B. Pispisa, *Biophys. J.*, 2005, **88**, 3411–3421.
24 N. Zhan, G. Palui, A. Kapur, V. Palomo, P. E. Dawson and H. Mattoussi, *J. Am. Chem. Soc.*, 2015, **137**, 16084–16097.
25 C. Toniolo, M. Crisma, F. Formaggio, C. Peggion, V. Monaco, C. Goulard, S. Rebuffat and B. Bodo, *J. Am. Chem. Soc.*, 1996, **118**, 4952–4958.

26 C.-P. Racz, G. Borodi, M. M. Pop, I. Kacso, S. Santa and M. Tomoaia-Cotisel, *Acta Crystallogr., Sect. B: Struct. Sci.*, 2012, **68**, 164–170.
27 C. Rentier, G. Pacini, F. Nuti, E. Peroni, P. Rovero and A. M. Papini, *J. Pept. Sci.*, 2015, **21**, 408–414.
28 L. A. Carpino, *J. Am. Chem. Soc.*, 1993, **115**, 4397–4398.
29 G. Sauerbrey, *Z. Phys.*, 1959, **55**, 206–222.
30 M. Rodahl, F. Höök and B. Kasemo, *Anal. Chem.*, 1996, **68**, 2219–2227.
31 *Practical Surface Analysis: Auger and X-Ray Photoelectron Spectroscopy*, ed. D. Briggs and M. P. Seah, Wiley, New York, NY, 1990, vol. 1.
32 J. C. Powell and A. Jablonski, *Surf. Sci.*, 2001, **448**, L547–L552.
33 Y. W. Yang and L. J. Fan, *Langmuir*, 2002, **18**, 1157–1164.
34 E. Longo, K. Wright, M. Caruso, E. Gatto, A. Palleschi, M. Scarselli, M. De Crescenzi, M. Crisma, F. Formaggio, C. Toniolo and M. Venanzi, *Nanoscale*, 2015, **7**, 15495–15506.
35 T. Ishida, N. Choi, W. Mizutani, H. Tokumoto, I. Kojima, H. Azehara, H. Hokari, U. Akiba and M. Fujihira, *Langmuir*, 1999, **15**, 6799–6806.
36 E. Reimhult, F. Hook and B. Kasemo, *Langmuir*, 2003, **19**, 1681–1691.
37 C. A. Keller and B. Kasemo, *Biophys. J.*, 1998, **75**, 1397–2140.
38 A. A. Feiler, A. Sahlholm, T. Sandberg and K. D. Caldwell, *J. Colloid Interface Sci.*, 2007, **315**, 475–481.
39 C. Toniolo, M. Crisma, F. Formaggio, C. Peggion, R. F. Epand and R. M. Epand, *Cell. Mol. Life Sci.*, 2001, **58**, 1179–1188.
40 Y. Shai, *Biopolymers*, 2002, **66**, 236–248.
41 S. Bobone, Y. Gerelli, M. De Zotti, G. Bocchinfuso, A. Farrotti, B. Orioni, F. Sebastiani, E. Latter, J. Penfold, R. Senesi, F. Formaggio, A. Palleschi, C. Toniolo, G. Fragneto and L. Stella, *Biochim. Biophys. Acta, Biomembr.*, 2013, **1828**, 1013–1024.
42 M. M. F. Sciacca, D. Milardi, G. M. L. Messina, G. Marletta, J. R. Brender, A. Ramamoorthy and C. La Rosa, *Biophys. J.*, 2013, **104**, 173–184.
43 V. Früh, A. P. IJzerman and G. Siegal, *Chem. Rev.*, 2011, **111**, 640–656.
44 B. Jose, C. T. Mallon, R. J. Forster, C. Blackledge and T. E. Keyes, *Chem. Commun.*, 2011, **47**, 12530–12532.
45 D. Japrung, J. Dogan, K. J. Freedman, A. Nadzeyka, S. Bauerdick, T. Albrecht, M. J. Kim, P. Jemth and J. B. Edel, *Anal. Chem.*, 2013, **85**, 2449–2456.